Instituto de Física
Universidade de São Paulo

Determination of the ^{12}C nuclear density through heavy-ion elastic scattering experiments

Gasques, L.R.[a] ; Chamon, L.C.[a]; Silva, C.P.[a]; Pereira, D.[a]; Alvarez, M.A.G.[a]; Rossi Jr., E.S.[a]; Likhachev, V.P.[b]; Carlson, B.V.[c]; De Conti, C.[c]

[a] Departamento de Física Nuclear, Instituto de Física da Universidade de São Paulo Caixa Postal 66318, 05315-970, São Paulo, SP,Brazil

[b] Departamento de Física Experimental, Instituto de Física da Universidade de São Paulo, Caixa Postal 66318, 05315-970 SP,Brazil

[c] Departamento de Física, Instituto Tecnológico de Aeronáutica, Centro Técnico Aeroespacial, São José dos Campos, SP, Brasil

Publicação IF - 1536/2002

Determination of the ^{12}C nuclear density through heavy-ion elastic scattering experiments.

L. R. Gasques[a], L. C. Chamon[a], C. P. Silva[a], D. Pereira[a], M. A. G. Alvarez[a], E. S. Rossi Jr.[a], V. P. Likhachev[b], B. V. Carlson[c] and C. De Conti[c].

[a] *Departamento de Física Nuclear, Instituto de Física da Universidade de São Paulo, Caixa Postal 66318, 05315-970, São Paulo, SP, Brazil.*

[b] *Departamento de Física Experimental, Instituto de Física da Universidade de São Paulo, Caixa Postal 66318, 05315-970, São Paulo, SP, Brazil.*

[c] *Departamento de Física, Instituto Tecnológico de Aeronáutica, Centro Técnico Aeroespacial, São José dos Campos, SP, Brazil.*

Precise elastic scattering differential cross sections have been measured for the $^{12}C + {}^{58}Ni,{}^{208}Pb$ systems at sub-barrier energies. The corresponding bare potentials have been determined at interaction distances larger than the respective barrier radii, and the results have been compared with those from an early extensive systematics for the nuclear potential. The present data have been combined with others for the $^{12}C + {}^{12}C,{}^{208}Pb$ systems at intermediate energies, in order to extract the ^{12}C ground-state nuclear density through an unfolding method.

PACS: 24.10.Ht, 21.10.Ft, 21.10.Gv
Keywords: Heavy-ion nuclear potential. Nuclear density.

1. Introduction

In this work, we present elastic scattering differential cross sections for the $^{12}C + {}^{58}Ni,{}^{208}Pb$ systems at sub-barrier energies. One of the purposes of the experiments was the determination of the corresponding nuclear potentials in a surface region near the respective barrier radii. The method was earlier applied to several systems involving the ^{16}O nucleus as projectile [1–4]. As discussed in these previous works, the imaginary part of the optical potential is negligible at sub-barrier energies due to the corresponding very small reaction cross sections. Thus, provided that a realistic shape in the surface region is assumed for the potential, the elastic scattering data analysis in this sub-barrier energy region unambiguously determines the real part of the interaction. The optical potential is composed of the bare and polarization potentials, the latter containing the contribution arising from nonelastic couplings. The real part of the polarization has been estimated earlier [1–3] through extensive coupled-channel calculations for the ^{16}O sub-barrier data set, and represents about 10% in comparison with the bare interaction. A quite complete coupled-channel calculation has been performed also for the $^{12}C + {}^{208}Pb$ system [5], and a good description of elastic, inelastic, transfer and fusion cross section data has been obtained for energies above the barrier. An extrapolation of the calculation (see Fig. 8 of Ref. [5]) to $54.5 \leq E_{Lab} \leq 57\ MeV$, an energy region which corresponds to the data of the present work, indicates that the polarization represents about 13% of the real part of the optical potential. Therefore, it is reasonable to assume that the experimentally extracted potential strengths for the $^{12}C + {}^{58}Ni,{}^{208}Pb$ systems at sub-barrier energies can be associated to the bare potential within about 10% precision.

In a recent work [6], an extensive systematics of optical potential strengths extracted from heavy-ion elastic scattering data analyses at low and intermediate energies was presented. The energy-dependence of the nuclear potential has been accounted for within a model based on the nonlocal nature of the interaction [6–9]. The systematics indicates that the heavy-ion potential can be described in a global way, through a double-folding shape which basically presents a simple dependence only on the number of nucleons of the colliding nuclei. The results for the nuclear potential of the $^{12}C + {}^{58}Ni,{}^{208}Pb$ systems obtained in the present work are in good agreement with such systematics for the bare interaction.

If the nonlocal model is assumed for the interaction, an unfolding method can be used to extract ground-state nuclear densities from heavy-ion elastic scattering data analyses. The method has been successfully applied in the experimental determination of densities for the $^{16,18}O$ nuclei [10]. In the present work, we apply the same procedure in the data analyses for the $^{12}C + {}^{58}Ni,{}^{208}Pb$ systems at sub-barrier energies, with the aim of obtaining the ^{12}C nuclear density at the surface region. The method is extended to the $^{12}C + {}^{12}C,{}^{208}Pb$ systems at intermediate energies, and in this case information about the ^{12}C density at much inner distances is obtained.

The paper is organized as follows. In Section 2, we present the experimental results and the determination of the

bare potential strengths from optical model data analyses for the $^{12}C + {}^{58}Ni,{}^{208}Pb$ systems. A brief summary of the nonlocal model, and a comparison between the present results and the early systematics for the nuclear potential are contained in Section 3. The extraction of the ^{12}C density and the limitations of the method are discussed in details in Section 4. Section 5 contains the main conclusions.

2. Experimental results and data analysis

The measurements were made at the São Paulo 8UD Pelletron Accelerator, Brazil. The detecting system has already been described in Ref. [1]. The thickness of the targets were about 60 $\mu g/cm^2$. Fig. 1 exhibits the elastic scattering cross sections for the $^{12}C + {}^{58}Ni,{}^{208}Pb$ systems in several sub-barrier energies.

In the optical model calculations, we have adopted a procedure similar to that described in the analysis of the sub-barrier data for the $^{16}O + {}^{58,60,62,64}Ni$, ^{88}Sr, $^{90,92}Zr$, ^{92}Mo, ^{120}Sn, ^{138}Ba, ^{208}Pb systems [1–4]. We have adopted a Woods-Saxon shape for the optical potential, with an inner imaginary part which takes into account the rather small internal absorption from barrier penetration. The values assumed for the parameters of the imaginary part of the potential result in very small strengths at the surface region. This procedure must be adopted in the sub-barrier data analysis due to the negligible cross sections of peripheral reaction channels. Concerning depth variations of this absorptive potential, no sensitivity in the elastic scattering cross section predictions has been detected. The radius parameters of the real part of the optical potential were fixed at $r_0(A_1^{1/3} + A_2^{1/3})$, with $r_0 = 1.06\ fm$, and the depth and diffuseness parameters were searched for the best data fits. For each angular distribution, we have found a family of potentials which give equivalent fits. These potentials cross (see Fig. 2) at a particular distance R_S, hereafter referred as the sensitivity radius.

The heavy-ion elastic scattering is sensitive to averages of the potential over distances comparable to the wavelength of the relative motion; therefore the results for sharply-defined sensitivity radii present some dependence on the shape assumed for the real part of the optical potential [11]. In most cases, including those of the present work, the scattering of heavy-ions is sensitive only to the potential for a very restricted range of surface distances around the sensitivity radius. In this region, a realistic potential, such as the double-folding, should present approximately an exponential shape with diffuseness values around 0.6 fm [12]. Thus, in order to avoid ambiguities in the potential determination, we have assumed a realistic shape for the potential in the surface region. Indeed, the exponential behavior with realistic diffuseness values is presented by the Woods-Saxon potential adopted in our analyses (see Fig. 2).

The sensitivity radius is energy-dependent (see Fig. 2), because at sub-barrier energies it is related to the classical turning point. We have used this fact to characterize the nuclear potential in the surface region (see Fig. 3). For such large interaction distances, the shape of the potential is nearly an exponential (solid lines in Fig. 3), with a diffuseness value about 0.64 fm. Similar behavior has been observed for systems with ^{16}O as the projectile [1–4]. The nuclear potentials equal 1 MeV at $R = 9.7$ fm and $R = 12.5$ fm (see Fig. 3) for the $^{12}C + {}^{58}Ni$ and $^{12}C + {}^{208}Pb$ systems, respectively. As discussed in the next Section, this difference between the nuclear potentials is directly connected with the corresponding different densities of the ^{58}Ni and ^{208}Pb nuclei.

3. Comparison with the nonlocal model

The elastic scattering data analyses for different systems in a very large energy range have resulted in phenomenological optical potentials with significant dependence on the bombarding energies [13]. Several theoretical models have been developed to account for this energy-dependence; one of them associates this dependence with nonlocal quantum effects related to the exchange of nucleons between target and projectile [6–9]. Within this model, the bare interaction V_N is connected with the folding potential V_F through

$$V_N(R,E) \approx V_F(R)\ e^{-4v^2/c^2}\ , \tag{1}$$

where c is the speed of light and v is the local relative speed between the nuclei,

$$v^2(R,E) = \frac{2}{\mu}\left[E - V_C(R) - V_N(R,E)\right]\ . \tag{2}$$

For the Coulomb interaction, V_C, we have used the expression for the double sharp cutoff potential [14].

The folding potential depends on the densities of the two partners in the collision

$$V_F(R) = \int \rho_1(r_1)\ \rho_2(r_2)\ u_0(\vec{R} - \vec{r_1} + \vec{r_2})\ d\vec{r_1}\ d\vec{r_2}\ . \tag{3}$$

With the aim of providing a global description of the nuclear interaction, in Ref. [6] a systematization of nuclear densities has been proposed, based on an extensive study involving charge distributions extracted from electron scattering experiments and theoretical densities calculated through the Dirac-Hartree-Bogoliubov model. This study has indicated that the two-parameter Fermi (2pF) distribution can be adopted to describe the nuclear densities, and an useful distinction between nucleon and matter distributions has been made. The radii of the 2pF distributions are well described by

$$R_i = 1.31\, A_i^{1/3} - 0.84\, fm\,, \tag{4}$$

where A is the number of nucleons of the nucleus. The nucleon and matter densities present average diffuseness values $a_N = 0.50$ fm and $a_M = 0.56$ fm, respectively. Due to effects of the structure of the nuclei, along the table of stable nuclides the R_i and a parameters vary around the corresponding average values . However, concerning the nuclear potential, the effects of the structure of the nuclei are mostly present at the surface and mainly related only to the diffuseness parameter [6].

Within this context, an extensive systematization of optical potential strengths extracted from heavy-ion elastic scattering data analyses at low and intermediate energies was performed [6]. The experimental potential strengths have been described within 25% precision, by combining Eqs. 1 and 3 through two different and equivalent methods. In the first alternative, the double-folding potential is treated in the usual interpretation [12]: the nucleon densities and an effective nucleon-nucleon interaction for $u_0(\vec{r})$ are adopted in Eq. 3. The standard M3Y interaction "frozen" at 10 MeV/nucleon [6,8] has been assumed for the effective nucleon-nucleon interaction. In the other alternative, the matter densities are adopted in Eq. 3, with a zero-range delta function assumed for $u_0(\vec{r})$:

$$u_0(\vec{r}) = V_0\, \delta(\vec{r})\,, \tag{5}$$

with $V_0 = -456$ MeV fm^3. This zero-range alternative is interesting because it results in approximate analytical expressions for the folding potential [6]. For example, in the surface region

$$V_F(R \geq R_1 + R_2) \approx V_0\, \rho_{01}\, \rho_{02}\, \pi a_M^2\, \mathcal{R}\, g(\tau)\, (1 + s/a_M)\, e^{-s/a_M}\,, \tag{6}$$

with $s = R - (R_1 + R_2)$, $\mathcal{R} = 2R_1R_2/(R_1 + R_2)$, $\tau = s/\mathcal{R}$. The ρ_{0i} are obtained from the normalization of the densities

$$4\pi \int_0^\infty \frac{\rho_{0i}}{1 + e^{(r-R_i)/a_M}}\, r^2\, dr = A_i\,, \tag{7}$$

and the function g is defined by:

$$g(\tau) = \frac{1 + \tau + \tau^2\zeta/3 + a_M/\mathcal{R} + (a_M/\mathcal{R} + 1/2)\, e^{-s/a_M}}{1 + \zeta\tau}\,, \tag{8}$$

$\zeta = \mathcal{R}/(R_1 + R_2)$.

Expression 1 has accounted for the energy-dependence of experimentally extracted potential strengths for a large number of different systems in a very wide energy range [6–9]. At sub-barrier energies and for radii close to the barrier radius, Eq. 1 indicates that $V_N \approx V_F$. In order to compare potentials from different systems, we have defined a reduced quantity, V_{red}, which removes the dependence of the sub-barrier potential strengths on the radii of the nuclei.

$$V_{red} = \frac{V_N}{V_0\, \rho_{01}\, \rho_{02}\, \mathcal{R}\, g(\tau)} \tag{9}$$

Taking into account Eqs. 6 and 9, the reduced potential should be a universal function of s

$$V_{red}(s \geq 0) \approx \pi a_M^2\, (1 + s/a_M)\, e^{-s/a_M}\,, \tag{10}$$

with the matter diffuseness approximately system-independent and close to the average value $a_M \approx 0.56$ fm [6].

The experimental reduced potential strengths for the ^{12}C + ^{58}Ni,^{208}Pb systems, calculated through Eq. 9, are in good agreement (see Fig. 4) with the predictions (Eq. 10 with $a_M = 0.56$ fm) of the early systematics for the bare potential. Assuming the nonlocal model with the densities proposed in such a systematics, good predictions for the elastic scattering cross sections are obtained (see the solid lines in Fig. 1).

In order to extend the analysis to higher energies, experimental elastic scattering angular distributions (from Refs. [15–17]) at several intermediate energies for the ^{12}C + ^{12}C,^{208}Pb systems have been included in our study. In the

sub-barrier case the imaginary potential used in the optical model calculations is based on very fundamental ground: the lack of surface absorption. Provided this condition is assumed, the results of the analyses at sub-barrier energies are independent on the parameters adopted for the imaginary potential. With the purpose of treating the absorptive part of the potential within a fundamental context also for intermediate energies, we have assumed (Eq. 11) the Lax-type interaction with Pauli blocking [18], which is the single-scattering term of the Glauber multiple scattering theory [19]

$$W(R,E) = -\frac{E}{k_N}\,\sigma_T^{NN}(E)\int \rho_1(|\vec{R}-\vec{r}|)\,\rho_2(r)\,d\vec{r}\,, \tag{11}$$

where $\sigma_T^{NN}(E)$ is the average nucleon-nucleon total cross section. In Fig. 5, a comparison between data and theoretical predictions (solid lines) for the angular distributions at intermediate energies is presented. Again we have assumed the nonlocal model for the real part of the interaction with the densities proposed in the systematics of Ref. [6]. Although the calculated cross section shows stronger oscillatory behavior, the magnitude, however, is in reasonable agreement with the data. Part of the theoretical oscillatory pattern could be damped in the data due to the angular aperture of the collimation system used in the experiments. We point out that no adjustable parameter has been used in either of the real and imaginary parts of the potential. It must be also remembered that only the single-scattering term of the multiple scattering series of Glauber has been included in the absorptive part of the potential, although higher order terms are quite likely to contribute significantly to the cross section. As we showed before [8], better fits can be obtained using a Woods-Saxon shape for the imaginary potential with three adjustable parameters. However, we regard the present approach as more fundamental.

4. Determination of the ^{12}C nuclear density

As we have discussed in Section 3, the experimentally extracted potential strengths for the ^{12}C + ^{58}Ni,^{208}Pb systems are compatible with the systematics for the nuclear potential of Ref. [6]. That systematics is based on densities with the shape of Fermi distributions, radii obtained from Eq. 4, and average diffuseness values $a_M = 0.56$ fm and $a_N = 0.50$ fm for the matter and nucleon distributions, respectively. In this sense, the analysis presented in Section 3 provides information about the nuclear densities of the partners in the collision. In this Section, we present another form of analysing the same set of cross section data, which determines the densities in a more direct manner than that of Section 3. If the nonlocal model is assumed for the heavy-ion interaction and the density of one nucleus is known, an unfolding method can be used to extract the density of the other nucleus from the elastic scattering data analyses. In Fig. 6, we compare the data (from Ref. [20–22]) with predictions for electron scattering cross sections on several nuclei. In the theoretical calculations, we have used charge distributions derived from the Dirac-Hartree-Bogoliubov (DHB) model [23]. The predictions are in good agreement with the data for the heavier nuclei, but discrepancies are observed for the ^{12}C and ^{16}O. This fact is an indication that the heavier the nucleus is, the more realistic is the theoretical density calculated through the DHB model. Therefore, we consider that the ^{58}Ni and ^{208}Pb densities are well described by the DHB calculations, and we have used the unfolding method to determine the ^{12}C nuclear density.

In this Section, the double-folding potential is considered in the usual interpretation: the nucleon densities and the M3Y effective nucleon-nucleon interaction are adopted in Eq. 3. The ^{12}C density is extracted from data analyses within a procedure similar to that used in the determination of potential strengths at the sensitivity radii. We have assumed the Fermi distribution to describe the ^{12}C nucleon density, with diffuseness (a_N) and radius (R_i) searched for the best data fits, and with the ρ_{0i} parameter determined by the normalization condition (Eq. 7). The real part of the optical potential is obtained from Eqs. 1 and 3, and has no adjustable parameters except those (a_N and R_i) connected only with the quantity to be determined: the ^{12}C nucleon density. For each angular distribution, we have found a family of densities which give equivalent data fits. These densities cross at two particular radii (see Fig. 7 - Top), and we associate only one of these radii to the sensitivity radius (r_S) for the density. To choose r_S, we have used the notch test (Fig. 7 - Bottom), in which a spline with a gaussian shape is included in the ^{12}C density, and the variation of the chi-square is studied as a function of the position of this perturbation. The crossing chosen as the sensitivity radius is that closest to the center of the region which affects significantly the elastic scattering data fit.

The determination of the error bar for the density at the sensitivity radius is illustrated in Fig. 8 for a particular elastic scattering angular distribution. At r_S the data extracted density value does not depend on the diffuseness assumed for the distribution. Thus, the dependence of the total chi-square on R_i is studied for a fixed a_N value, and the parameters that correspond to the minimum value χ^2_{min} and to $\chi^2_{min} + \chi^2_{min}/n$ are found (see the determination of R_{0min}, R_{0-} and R_{0+} in Fig. 8a); n is the number of experimental data points of the angular distribution. Fig. 8b presents the Fermi distributions for the R_{0min}, R_{0-} and R_{0+} values, and the respective determination of the error bar for the density at r_S.

Similar to the case of the potential determination, the sensitivity radius for the density is energy-dependent and this fact allows the characterization of the density over a large range of distances. Fig. 9a contains the ^{12}C experimental nucleon density values at the corresponding sensitivity radii obtained from data analyses of several angular distributions. The sub-barrier elastic scattering data gives information about the density at the surface region, while inner distances are probed through the data at intermediate energies. We point out that data analyses for different systems provide consistent similar results for the ^{12}C density. The theoretical prediction from the DHB model (see Fig. 9) does not match the experimental results at the surface region. Taking into account the discussion about the nuclear potential of Section 3, another consistent result of our analysis is the agreement (see Fig. 9) between the Fermi distribution that has been assumed in the potential systematics of Ref. [6] and the experimental density values from sub-barrier data analyses. We mention that other experimental data for the ^{12}C density in the region $2 \leq r \leq 4$ fm could be found through the analyses of other angular distributions in an energy region in between the sub-barrier and intermediate energies analysed in the present work, but in this case the imaginary potential would have adjustable parameters and the reliability of the results for the density should be studied much more carefully.

Now we evaluate the effects of two possible sources of systematical errors in the density determination: the polarization potential and the shape of the density distribution. As discussed in Section 1, coupled-channel calculations have indicated that the polarization represents about 10% of the real part of the optical potential at sub-barrier energies. In the data analysis, we have neglected the polarization and associated the real part of the optical potential only with the bare interaction, which is directly proportional to the nuclear densities. Thus, a systematical error of about 10% is expected in our results for the density in the surface region, due to the procedure of neglecting the polarization potential for sub-barrier energies. The threshold anomaly [24] indicates that the contribution of the polarization to the real part of the optical potential should be more significant in the region of the Coulomb barrier, so we estimate this contribution at intermediate energies (inner density distances) to be even less than 10%. Another source of systematical errors is the shape assumed for the density distribution. Similar to the case of the potential determination, the notch test indicates that the data fit is sensitive to a density region of width ($\sigma = 2.5\ fm$ - see Fig. 7) comparable to the wavelength of the relative motion. However, in contrast with the potential case, in such region ($2.5 \leq r \leq 5.0\ fm$) a realistic shape for the density may present significant difference of the pure exponential form (see Fig. 7). Therefore, one could expect some dependence of the results for the sensitivity radius on the shape adopted for the density distribution, particularly for intermediate energies in which inner distances are probed. Thus, in order to investigate the dependence of the method on the shape assumed for the ^{12}C distribution, we have also performed data analyses using the harmonic oscillator (HO) shape (Eq. 12), with two adjustable parameters (w and α).

$$\rho(r) = \rho_0 \left(1 + \alpha \frac{r^2}{w^2}\right) e^{-r^2/w^2} \tag{12}$$

The corresponding results for the densities at the sensitivity radii are presented in Fig. 9b. At the surface region an average difference of 22% between the HO and 2pF results has been found. Therefore, within this precision, our studies indicate that the results for the ^{12}C density at the surface region are rather independent on the model assumed for the shape of the distribution. The results from intermediate energies are more sensitive to the shape, but even in this case the different models (HO and 2pF) provide similar overall trends for the density.

As a further test of the consistency of our results for the ^{12}C density, in Fig. 6 we compare the data with predictions for electron scattering cross sections. In the theoretical calculations, we have obtained the ^{12}C charge distribution by folding the proton density of the nucleus (ρ_p) with the intrinsic charge distribution of the proton in free space (ρ_{chp})

$$\rho_{ch}(r) = \int \rho_p(\vec{r'})\ \rho_{chp}(\vec{r} - \vec{r'})\ d\vec{r'}\ , \tag{13}$$

where ρ_{chp} is an exponential with diffuseness $a_{chp} = 0.235$ fm. We have estimated the ^{12}C proton distribution as one half of the total (proton + neutron) nucleon distribution. The dashed line in Fig. 6 represents the results for the cross sections obtained by considering the 2pF distribution of Ref. [6] for the total ^{12}C density (solid lines in Fig. 9). Such results are much closer to the data than the DHB predictions.

5. Conclusion

In this work, we have presented elastic scattering data at sub-barrier energies for systems involving ^{12}C as projectile, and we have extended our studies to other data sets earlier obtained at intermediate energies. In our optical model data analysis, the imaginary part of the potential is based only on very fundamental grounds and has no adjustable parameters. The nonlocal model is assumed to describe the energy-dependence of the real part of the interaction,

which is connected to the folding potential through the very simple equation 1. Within this context and assuming the systematics of Ref. [6] for the nuclear densities, a reasonable prediction of the elastic scattering cross sections is obtained for the whole data set without the use of any adjustable parameter.

If the target densities are known, we have shown that the density of the projectile can be extracted from the data analysis in a direct procedure. The sub-barrier elastic scattering data gives information about the density at the surface region, while inner distances are probed through the data at intermediate energies. The results for the ^{12}C nuclear density are consistently independent on the target nucleus, and in reasonable agreement with the Fermi distribution resulting from the systematics of Ref. [6]. We estimate in 20% to 30% the overall systematical error in the density results, from two main sources: the polarization potential and the shape assumed for the density of the projectile. The method should be a powerful tool to determine densities of exotic nuclei, particularly at the surface region where the difference between densities of exotic and neighbouring stable nuclei is much emphasized.

This work was partially supported by Financiadora de Estudos e Projetos (FINEP), Fundação de Amparo à Pesquisa do Estado de São Paulo (FAPESP), and Conselho Nacional de Desenvolvimento Científico e Tecnológico (CNPq).

---

[1] L. C. Chamon, D. Pereira, E. S. Rossi Jr., C. P. Silva, R. Lichtenthaler Filho and L. C. Gomes, Nucl. Phys. **A582**, 305 (1995).
[2] L. C. Chamon, D. Pereira, E. S. Rossi Jr., C. P. Silva, H. Dias, L. Losano and C. A. P. Ceneviva, Nucl. Phys. **A597**, 253 (1996).
[3] M. A. G. Alvarez, L. C. Chamon, D. Pereira, E. S. Rossi Jr., C. P. Silva, L. R. Gasques, H. Dias and M. O. Roos, Nucl. Phys. **A656**, 187 (1999).
[4] C. P. Silva, M. A. G. Alvarez, L. C. Chamon, D. Pereira, M. N. Rao, E. S. Rossi Jr., L. R. Gasques, M. A. E. Santo, R. M. Anjos, J. Lubian, P. R. S. Gomes, C. Muri, B. V. Carlson, S. Kailas, A. Chatterjee, P. Singh, A. Shivastava, K. Mahata and S. Santra, Nucl. Phys. **A679**, 287 (2001).
[5] S. Santra, P. Singh, S. Kailas, A. Chatterjee, A. Shrivastava and K. Mahata, Phys. Rev. **C64**, 024602 (2001).
[6] L. C. Chamon, B. V. Carlson, L. R. Gasques, D. Pereira, C. De Conti, M. A. G. Alvarez, M. S. Hussein, M. A. Candido Ribeiro, E. S. Rossi Jr. and C. P. Silva, submitted to Phys. Rev. **C**.
[7] M. A. C. Ribeiro, L. C. Chamon, D. Pereira, M. S. Hussein and D. Galetti, Phys. Rev. Lett. **78**, 3270 (1997).
[8] L. C. Chamon, D. Pereira, M. S. Hussein M. A. C. Ribeiro and D. Galetti, Phys. Rev. Lett. **79**, 5218 (1997).
[9] L. C. Chamon, D. Pereira and M. S. Hussein, Phys. Rev. **C58**, 576 (1998).
[10] M. A. G. Alvarez, E. S. Rossi Jr., C. P. Silva, L. R. Gasques, L. C. Chamon, D. Pereira, M. N. Rao, B. V. Carlson, C. De Conti, R. M. Anjos, P. R. S. Gomes, J. Lubian, S. Kailas, A. Chatterjee and P. Singh, Phys. Rev. **C65**, 014602 (2002).
[11] M. H. Macfarlane and S. C. Pieper, Phys. Lett. **103B**, 169 (1981).
[12] G. R. Satchler and W. G. Love, Phys. Rep. **55**, 183 (1979).
[13] M. E. Brandan and G. R. Satchler, Phys. Rep. **285**, 142 (1992), and references therein.
[14] R. M. Devries and M. R. Clover, Nucl. Phys. **A243**, 528 (1975).
[15] J. Y. Hostachy, M. Buenerd, J. Chauvin, D. Lebrun, Ph. Martin, J. C. Lugol, L. Papineau, P. Roussel, N. Alamanos, J. Arviex and C. Cerruti, Nucl. Phys. **A490**, 441 (1988).
[16] M. Buenerd, A. Lounis, J. Chauvin, D. Lebrun, P. Martin, G. Duhamel, J. C. Gondrand and P. de Saintignon, Nucl. Phys. **A424**, 313 (1984).
[17] M. Buenerd, J. Pinston, J. Cole, C. Guet, D. Lebrun, J. M. Loiseaux, P. Martin, E. Monnand, J. Mougey, H. Nifenecker, R. Ost, P. Perrin, Ch. Ristori, P. de Saintgnon, F. Schussler, L. Carlen, H. A. Gustafsson, B. Jakobsson, T. Johansson, G. Jonsson, J. Krumlinde, I. Otterlund, H. Ryde, B. Schroder, G. Tibell, J. B. Bondorf and O. B. Nielsen, Phys. Lett. **102B**, 242 (1981).
[18] See, e.g., M. S. Hussein, R. A. Rego and C. A. Bertulani, Phys. Rep. **201**, 279 (1991).
[19] R. J. Glauber, Lectures in theoretical physics, (Interscience, New York, 1959) vol 1, p. 315; High-energy physics and nuclear structure, (Plenum, New York, 1970), p. 207.
[20] J. R. Ficenec, W. P. Trower, J. Heisenberg and I. Sick, Phys. Lett. **B32**, 460 (1970).
[21] I. Sick and J. S. MacCarthy, Nucl. Phys. **A150**, 631 (1970).
[22] B. Frois, J. B. Bellicard, J. M. Cavedon, M. Huet, P. Leconte, P. Ludeau, A. Nakada and Phan Zuan Hô, Phys. Rev. Lett **38**, 152 (1977).
[23] B. V. Carlson and D. Hirata, Phys. Rev. **C62**, 054310 (2000).
[24] G. R. Satchler, Phys. Rep. **199**, 147 (1991).

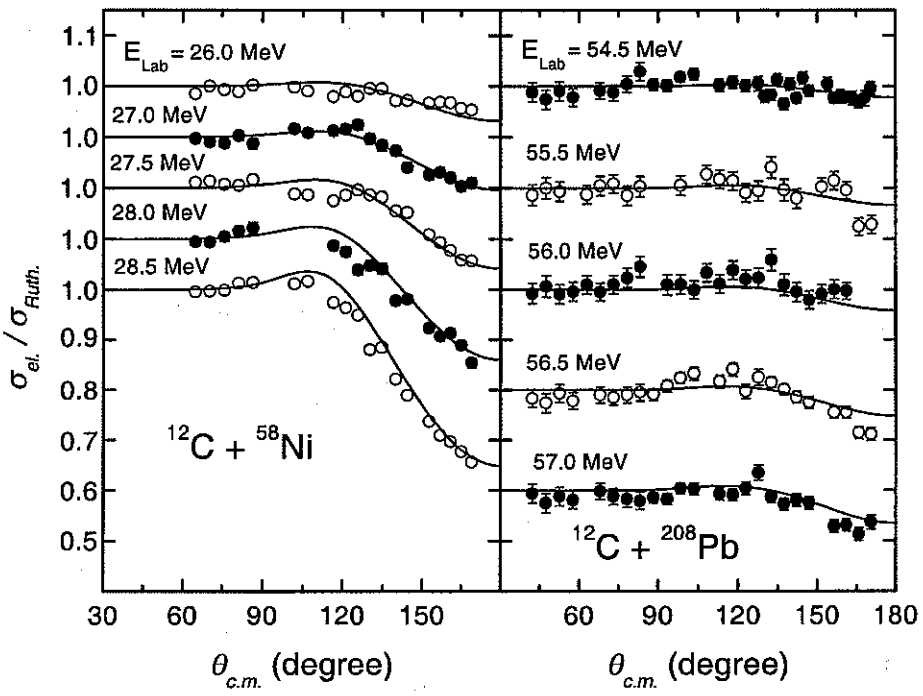

FIG. 1. Elastic scattering angular distributions for the $^{12}C + ^{58}Ni$, ^{208}Pb systems at several sub-barrier energies. The solid lines represent optical model predictions, in which the nonlocal model is assumed for the real part of the interaction. Note that the cross section is represented in a linear scale.

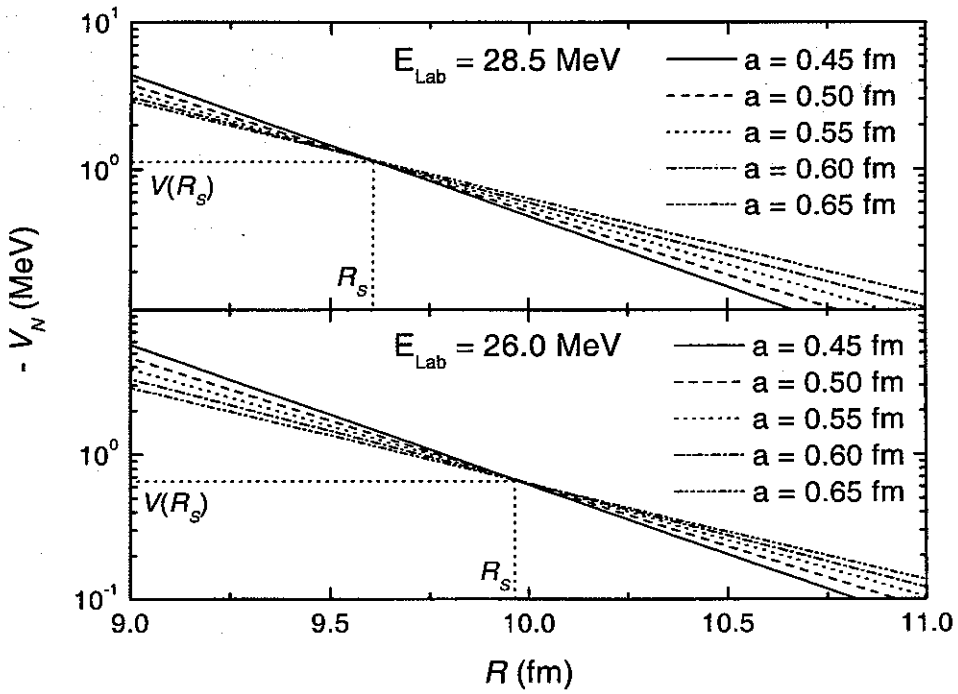

FIG. 2. The real part of the optical potential for the $^{12}C + ^{58}Ni$ system at two different energies, as obtained by optical model data fits for several values of the diffuseness parameter. The potentials cross at the sensitivity radii, R_S, where the corresponding potential strengths are determined without ambiguities.

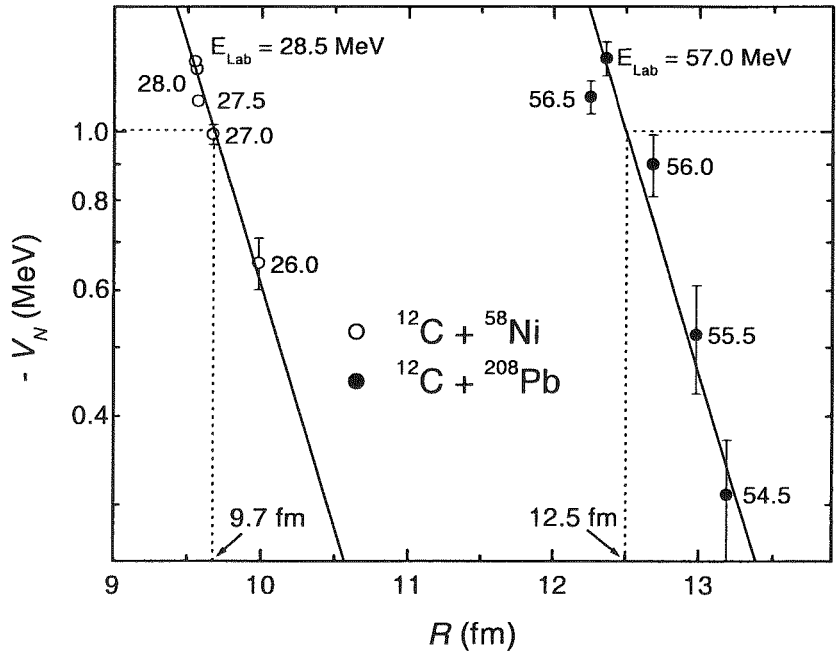

FIG. 3. The nuclear potential strength as a function of the sensitivity radius for the ^{12}C + ^{58}Ni, ^{208}Pb systems. The bombarding energies of the elastic scattering angular distributions in which the sensitivity radii have been determined are indicated in the figure. The solid lines represent exponentials with diffuseness value 0.64 fm. The radii at which the potentials equal 1 MeV are indicated in the figure.

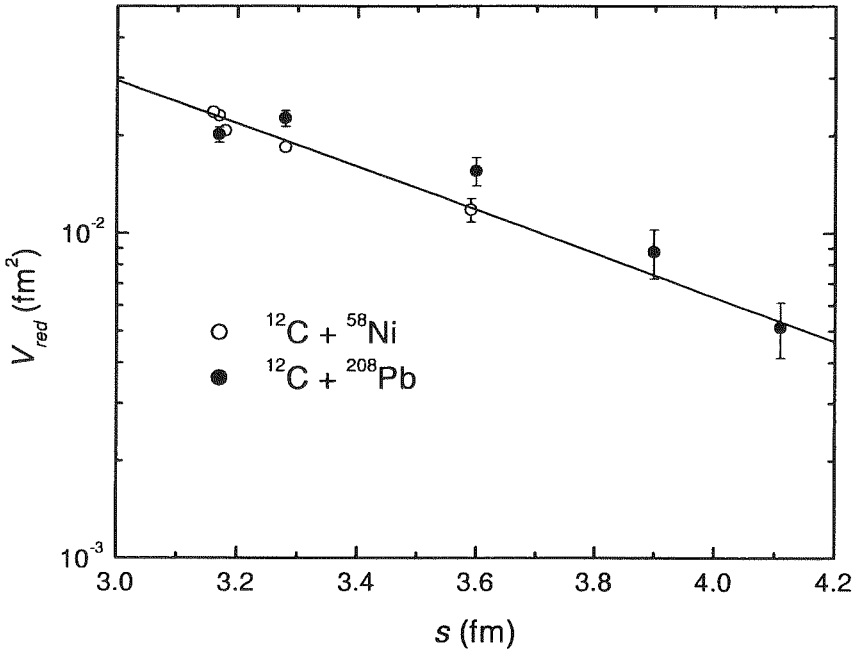

FIG. 4. The experimental reduced potential strength as a function of the reduced distance, s, for the ^{12}C + ^{58}Ni, ^{208}Pb systems. The solid line represents the theoretical prediction, Eq. 10 with $a_M = 0.56$ fm.

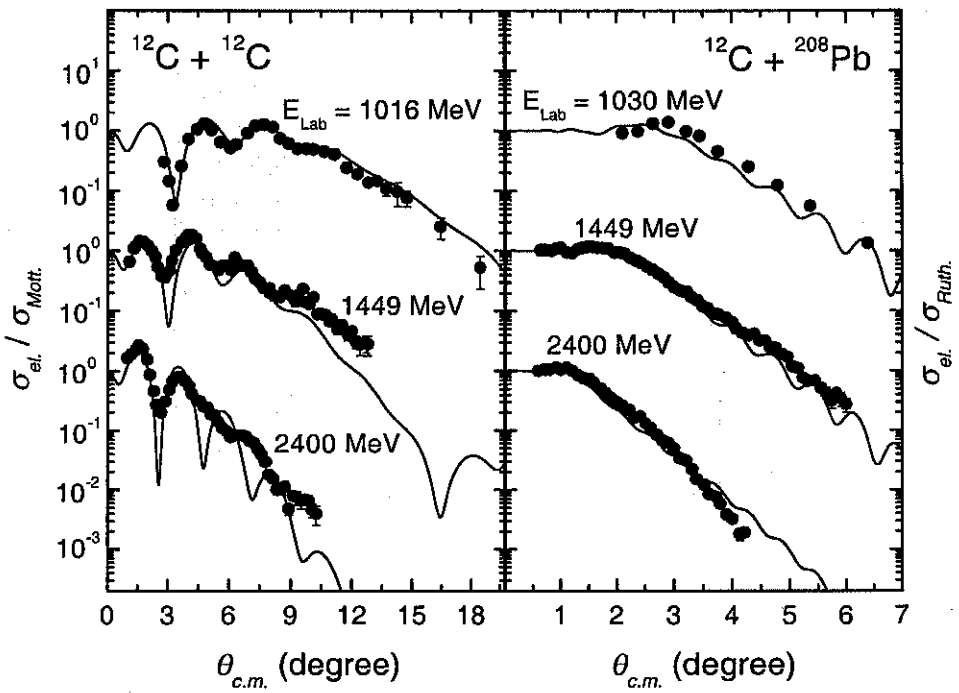

FIG. 5. Elastic scattering angular distributions for the $^{12}C + ^{12}C$, ^{208}Pb systems at several intermediate energies. The solid lines represent optical model predictions, in which the free-parameter nonlocal model and the Lax-type interaction are assumed for the real and imaginary parts of the potential, respectively.

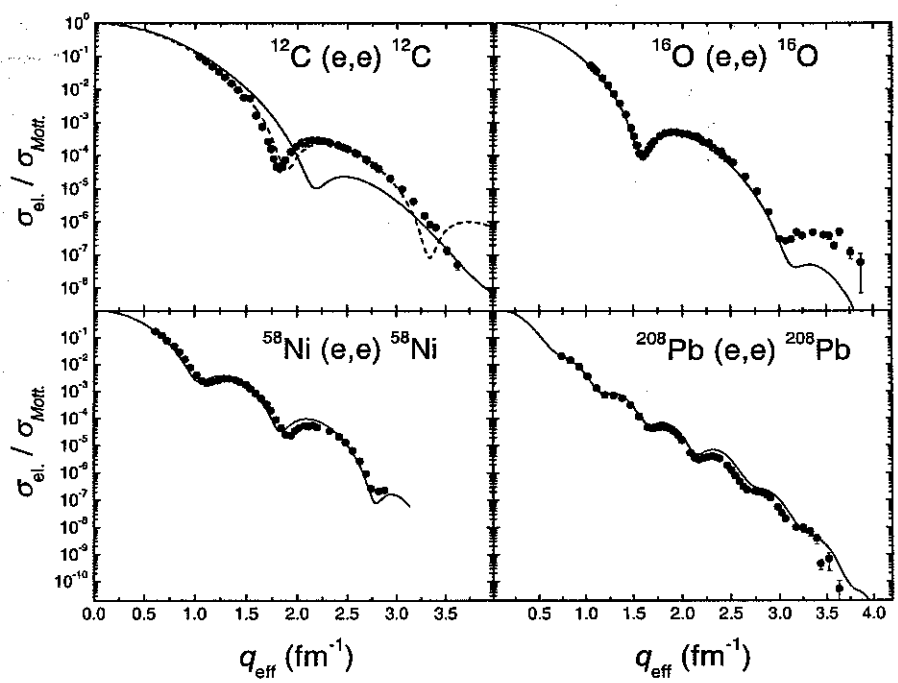

FIG. 6. Experimental electron scattering cross sections for the ^{12}C, ^{16}O, ^{58}Ni and ^{208}Pb nuclei as a function of the effective momentum transferred. The solid lines represent theoretical predictions using charge distributions derived from Dirac-Hartree-Bogoliubov calculations. The dashed line in the ^{12}C case represents calculations based on a 2pF distribution (see text for details).

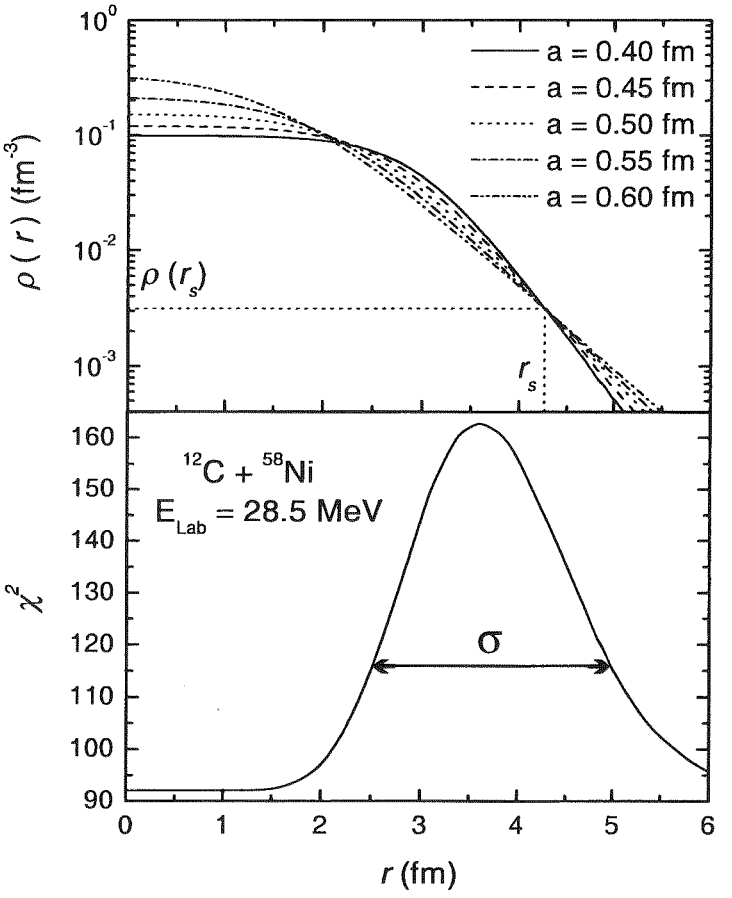

FIG. 7. (Top) - Example of the determination of the sensitivity radius, r_S, and the corresponding experimental value for the ^{12}C nucleon density, using two-parameter Fermi distributions which give equivalent data fits for the angular distribution of the ^{12}C + ^{58}Ni system at E_{Lab} = 28.5 MeV. (Bottom) - The sensitivity region for the ^{12}C nucleon density characterized by the notch test.

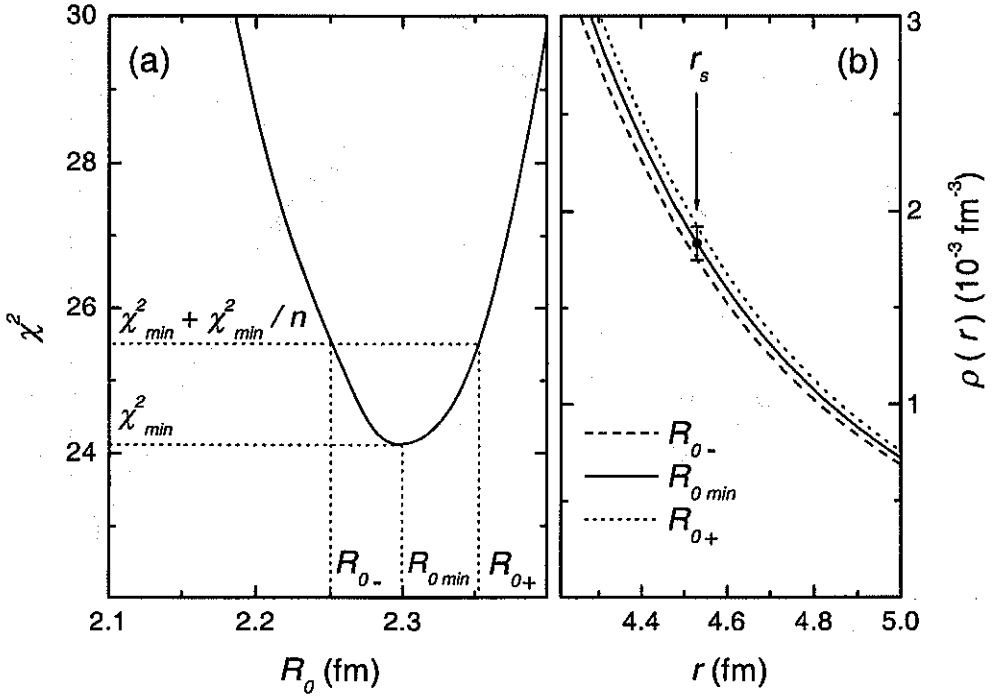

FIG. 8. The figure presents an example of the determination of the error bar for the ^{12}C density at r_S for the angular distribution of the ^{12}C + ^{58}Ni system at $E_{Lab} = 27$ MeV. (a) - The total chi-square as a function of the radius of the Fermi distribution for the fixed diffuseness parameter $a = 0.5$ fm, and the determination of the R_{0min}, R_{0-} and R_{0+} values. (b) - The Fermi distributions which correspond to the R_{0min}, R_{0-} and R_{0+} values, and the determination of the error bar for ρ at r_S.

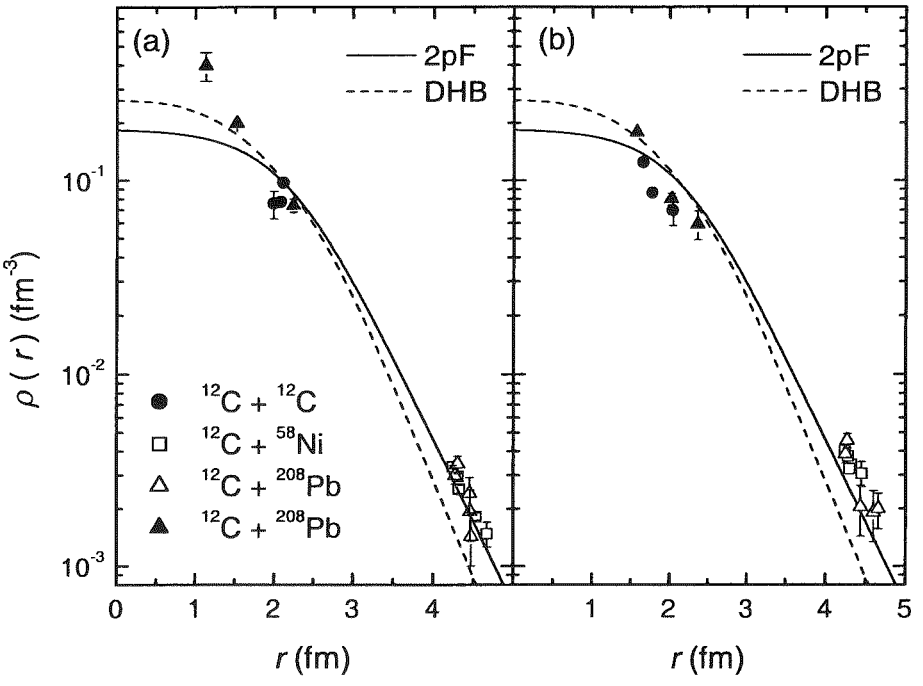

FIG. 9. Experimental nucleon density values for the ^{12}C nucleus, as obtained from elastic scattering data analyses for different heavy-ion systems at sub-barrier (open symbols) and intermediate (closed symbols) energies. Parts (a) and (b) of the figure concern the results of analyses considering the Fermi or Harmonic Oscillator shapes for the ^{12}C density, respectively. The lines correspond to theoretical Dirac-Hartree-Bogoliubov (DHB) calculations, and to the Fermi distribution (2pF) proposed in Ref. [6].